DOI: https://doi.org/10.2138/am-2020-7431. http://www.minsocam.org/

Revision 1

Contrasting compositions between phenocrystic and xenocrystic olivines in the Cenozoic basalts from central Mongolia: Constraints on source lithology and regional uplift

Yunying Zhang[1,2], Chao Yuan[2], Min Sun[1]*, Zongying Huang[2], Tserendash Narantsetseg[3], Zhongyuan Ren[2], Pengfei Li[2], Qinglin Zhang[2]

[1]Department of Earth Sciences, The University of Hong Kong, Pokfulam Road, Hong Kong, China

[2]State Key Laboratory of Isotope Geochemistry, Guangzhou Institute of Geochemistry, Chinese Academy of Sciences, Guangzhou 510640, China

[3]Institute of Paleontology and Geology, Mongolian Academy of Sciences, Ulaanbaatar 15160, Mongolia

* Corresponding author. Tel.: +852 28592194; fax: +852 25176912.
E-mail address: minsun@hku.hk (M. Sun).

ABSTRACT

Two Cenozoic prominent features are spatio-temporally associated in central Mongolia, i.e., the continental basalts and regional uplift, but their genesis and relationship remain unclear. This study presents major and trace element compositions for olivine phenocrysts and xenocrysts, as well as data of bulk-rock geochemistry and

Sr–Nd–Hf isotopes for the host basalts. The studied basalts mostly have trachybasalt compositions with high total alkali (Na_2O + K_2O = 5.1–8.2 wt%) contents and all display OIB-like trace element patterns (e.g., spikes of Ba, Nb and Ta and troughs of Th and U) and EM1-like Sr–Nd–Hf isotopic compositions. Compared to the partial melting products of mantle peridotite, these basaltic samples have higher FeO/MnO, Zn/Mn and Zn/Fe ratios. Meanwhile, phenocrystic olivines are featured by lower Ca, Mn, Mn/Zn and Mn/Fe but higher Ni than their counterparts in the peridotitic melts, indicating a pyroxenite-rich mantle source. The above geochemical data suggest that the source of the studied basalts was mainly made up of secondary pyroxenite produced by reaction of recycled oceanic crust with its ambient mantle peridotite. The calculated magma oxygen fugacities (ΔFMQ –0.26 to +0.42) and mantle melting temperatures (1343–1430°C) do not support a genetic link with the stagnant Pacific slab or with a deep mantle plume. Instead, the far-field effect of India–Eurasia convergence possibly tapped the upper asthenospheric mantle, subsequent melting of which gave rise to the dispersive Cenozoic basalts. On the other hand, the xenocrystic olivines exhibit zoned textures with high-Fo (up to 92) cores and low-Fo (down to 76) rims, reflecting the melt–rock interaction. Preservation of zoned olivine xenocrysts indicates rapid magma ascent and widespread melt–rock reaction in the mantle lithosphere, which may modify the rheology and accelerate the mechanical erosion of mantle lithosphere. Consequently, mass deficit in the lithosphere could have caused isostatic uplift of central Mongolia in the Cenozoic.

Keywords: Cenozoic continental basalts, Central Mongolia, Olivine chemistry, Pyroxenite, Regional uplift

INTRODUCTION

Cenozoic (~30 Ma to present) continental basalts are diffusely distributed in the central Asia (Fig. 1), and are dominated by alkaline basalts with subordinate tholeiites and show oceanic island basalt (OIB)-like trace element features (Johnson et al. 2005; Hunt et al. 2012; Ivanov et al. 2015; Zhang et al. 2019). These basalts are mainly concentrated in three volcanic provinces, namely the Transbaikalia province in south Siberia, the Hangai province in central Mongolia and the Gobi Altai province in south Mongolia (Barry et al. 2003). The petrogenesis for basalts in the Hangai province seems most mysterious, because (1) they are far from any active plate boundary, (2) they erupted within a rigid block lacking substantial lithospheric extension or rifting and (3) they formed over a long period of 30 Myrs without age progression (Ancuta et al. 2018). The unsolved mysteries primarily revolve around their magmatic source, i.e., lithospheric mantle or asthenospheric mantle (Barry et al. 2003; Hunt et al. 2012), and the associated geodynamic mechanism, i.e., mantle plume (Windley and Allen 1993; Yarmolyuk et al. 2015), lithospheric delamination (Hunt et al. 2012), Pacific subduction (Meng et al. 2018) or India–Eurasia collision (Cunningham 2001). The above debates are largely due to the short of knowledge on their source lithology and thermal–chemical conditions (e.g., T–fO_2), which are crucial to decipher the ultimate magma origin and geodynamic process.

On the other hand, the Hangai Mountains represent a 2×10^5 km^2 region of high elevation (>3500–4000 m) and low-relief and long-wavelength topography in central Mongolia (McDannell et al. 2018), which may create the arid climate of northern Gobi in central Asia (West et al. 2013; Caves et al. 2014). Based on apatite (U-Th)/He cooling ages, it has been suggested that the Hangai Mountains were uplifted mainly in the late Mesozoic as a result of the Jurassic–Cretaceous termination of the Mongol–Okhotsk orogeny (McDannell et al. 2018). Within the following Cenozoic era, the Hangai Mountains evolved into an entirely epeirogenic stage with modest surface uplift (Caves et al. 2014; Sahagian et al. 2016; Smith et al. 2016). Despite variable mechanisms for the later-stage (i.e., Cenozoic) uplift (e.g., localized mantle plume activity, underplated mafic cumulates, asthenospheric upwelling and lithospheric delamination; Windley and Allen 1993; Petit et al. 2002; Hunt et al. 2012; Chen et al. 2015), it is widely accepted that upper mantle dynamics necessarily played a critical role. This is in line with the indication that the long-wavelength topography is commonly related to the dynamic interaction between asthenosphere and lithosphere (Braun 2010).

Phenocrystic olivine is always the first silicate phase to crystallize from primary basaltic melts and thus could faithfully record information about the magma source (Foley et al. 2013), while xenocrystic olivine captured by basaltic magmas directly came from the mantle and may provide insights into the deep process such as asthenosphere–lithosphere interaction (De Hoog et al. 2010; Tollan et al. 2015). In this study, we report for the first time major and trace element compositions for these two types of olivines from the Cenozoic basalts in the Hangai Mountains. Combing with our newly obtained bulk-rock geochemistry and Sr–Nd–Hf isotopes, we aim to (1) characterize their mantle source lithology, (2) constrain the thermal–chemical conditions (T–fO_2) and (3) assess the possible role of asthenosphere–lithosphere interaction in the genesis of Cenozoic basalts and regional uplift.

GEOLOGICAL BACKGROUND AND SAMPLES

The Hangai region in central Mongolia is composed of Archean to Proterozoic basement (e.g., gneisses and schists), which is unconformably overlain by Paleozoic clastic sediments and was intensively intruded by Permian granitoids (Cunningham 2001; Badarch et al. 2002). The crustal and lithospheric thickness beneath this region have been estimated to be 44–50 km and 80–90 km, respectively (Barruol et al. 2008; Fullea et al. 2012). The post-Oligocene (30–25 Ma) uplift led the Cretaceous to Paleogene erosion surface to be domed to a maximum elevation of 4000 m, 2000 m above the average altitude of Mongolia (Walker et al. 2007, and references therein). Meanwhile, voluminous basalts with ages from 30 Ma to 5 ka and volume up to 2900 km^3 erupted throughout the period of uplift (Barry et al. 2003). The most voluminous phase (15–10 Ma) of basalts is distributed on the south and northeast Hangai, while the sporadic phase (>15 Ma) of basalts is predominantly located in the east Hangai (Fig. 2; Ancuta et al. 2018). The post-10 Ma basalts are suffused across much of the Hangai region, mainly in the east (e.g., Nuruu), central (e.g., Jargalant) and north (e.g., Tariat, Hanui, Togo and Orkhon) (Fig. 2). Geochemically, these basaltic rocks are mainly basanite, trachybasalt and basaltic trachyandesite, and show strong shoshonitic affinity (Savatenkov et al. 2010; Hunt et al. 2012).

Representative basaltic samples from central (i.e., Jargalant) and north (i.e., Tariat, Togo and Orkhon) Hangai were collected for geochemical investigation (see sample localities on Figure 2). Five, nine, four and ten basaltic samples were collected from the Jargalant, Tariat, Togo and Orkhon volcanic fields, respectively. The basaltic lavas in the Jargalant field occurred within the Vodorazdel'nyi graben and the upstream of the Chulut River (Savatenkov et al. 2010), and erupted mainly in the late Miocene (12.8–6.0 Ma) and subordinately in the Pliocene (4.7–2.5 Ma) (Ancuta et al. 2018). The Tariat volcanic field is exceptional for its abundance of crustal and mantle xenoliths (Ionov et al. 1994; Barry et al. 2003; Harris et al. 2010). Lavas erupted in the late Pleistocene, with ages between 0.5 and 0.1 Ma, are largely exposed along the Sumyn River and within half-grabens that now form the Chulut River channels, while lavas erupted in the late Miocene, with ages of ~5.9 Ma, mostly occur on both uplifted sides of the Chulut River. The Togo and Orkhon volcanic fields embrace the Selenga–Orkhon interfluve (Fig. 2). The basaltic lavas in the Togo field are geochronologically similar to those in the Tariat field, and can be subdivided into two episodes, namely the late Miocene (5.9–5.7 Ma) and late Pleistocene (~0.3 Ma), while lavas in the Orkhon field mainly formed during the late Pliocene (3.8–3.1 Ma).

All the samples of basalts in this study are gray black in color and porphyritic in texture. Megacrysts are mainly olivines with the majority as phenocrysts and the minority as xenocrysts. The phenocrystic olivines are subhedral to euhedral and typically 0.5–1.5 mm in size, while the xenocrystic olivines are generally 0.5–2.5 mm in size and are featured by irregular to subround shape and up to ~100 μm wide rims with regular embayments (Fig. 3). Moreover, abundant plagioclases are present as phenocrysts in some Jargalant basalts and minor megacrysts of phenocrystic clinopyroxene and xenocrystic orthopyroxene are found in the Orkhon basalts. The matrix is fine-grained and contains plagioclase, clinopyroxene, olivine and opaque minerals, and sometimes the plagioclase grains are well crystallized with length up to 0.5 mm.

ANALYTICAL METHODS

Bulk-rock major and trace element analyses were performed at the Wuhan Samplesolution Analytical Technology Co. Ltd. (Wuhan, China). Major oxides were analyzed by using a X-ray fluorescence spectrometer (Primus II, Rigaku, Japan) on fused glass beads, and the analytical precision was generally better than 2% based on the measurement of Chinese rock standard GBW07105. Trace elements, including rare earth element (REE), high field strength element (HFSE) and large ion lithophile element (LILE), were measured by using an Agilent 7700e inductively-coupled plasma mass spectrometer (ICP-MS) instrument. Rock powders (~50 mg) were digested using a HF + HNO_3 mixture in Teflon bombs, which were placed into stainless steel pressure jackets and then heated to 190 °C in an oven for over 24 hours. The USGS rock standards BHVO-2, AGV-2 and BCR-2 were run as unknown to monitor the data quality, and the precision was generally better than 6%. The obtained results for all the rock standards are presented in Table S1.

Bulk rock Sr–Nd–Hf isotopic analyses were conducted on a Micromass Isoprobe multi-collector (MC) ICP-MS instrument at the State Key Laboratory of Isotope Geochemistry, Guangzhou Institute of Geochemistry, Chinese Academy of Sciences (SKLIG GIG CAS). Analytical procedures are similar to those described in Wei et al. (2002), Li et al. (2006) and Wu et al. (2007). Measured $^{87}Sr/^{86}Sr$ and $^{143}Nd/^{144}Nd$ ratios were normalized to $^{86}Sr/^{88}Sr$ = 0.1194 and $^{146}Nd/^{144}Nd$ = 0.7219, respectively. During the analysis session for our samples, the measured values for the NBS987 Sr standard and JNdi-1 Nd standard were 0.710248 ± 20 (2σ) for $^{87}Sr/^{86}Sr$ and 0.512111 ± 12 (2σ) for $^{143}Nd/^{144}Nd$, respectively. These values are identical to the reported results (0.710244 ± 14 (2σ) for NBS987 Sr standard and 0.512115 ± 7 (2σ) for JNdi-1 Nd standard) (Tanaka et al. 2000; Elburg et al. 2005). The measured $^{176}Hf/^{177}Hf$ ratios were normalized to $^{179}Hf/^{177}Hf$ = 0.7325, and the reference standard JMC14374 was analyzed along with samples and gave $^{176}Hf/^{177}Hf$ = 0.282180 ± 8 (2σ), in accord with previously reported values of 0.282188 ± 17 (2σ) by Wu et al. (2007).

Mineral major elements were measured at the Key Laboratory of Mineralogy and Metallogeny in GIG CAS, and at the Department of Earth Sciences in the University of Hong Kong, by electron probe microanalysis (EPMA) using a JEOL JXA-8230 Superprobe. The analyses were carried out at a 15 kV accelerating voltage and a 20 nA beam current. The beam spot diameter was set at 1 μm for analysis. Relative analytical errors for olivines are estimated to be < 1% for major elements (SiO_2, FeO and MgO) and < 4% for minor elements (CaO, NiO and MnO). All analytical data were reduced using the ZAF correction routines and the analytical procedures are described in detail by Xing et al. (2017) and Li and Zhou (2018). Trace element compositions of minerals were analyzed at the Key Laboratory of Mineralogy and Metallogeny in GIG CAS, using the laser inductively (LA) ICP-MS technique (an Agilent 7500a ICP-MS system coupled with a Resonetic 193 nm ArF-excimer laser sampler). Laser ablation was undertaken at a constant energy 80 mJ and at 6 Hz. NIST SRM 610 glass was used as an external standard and GOR-132 glass was employed as an unknown sample and the SiO_2 contents measured by EPMA were used as an internal standard. Data reduction was performed by the ICPMSDataCal software (Liu et al. 2008), and analytical uncertainty is less than 10% (relative).

RESULTS

Bulk-rock geochemical compositions

Bulk rock major–trace element and Sr–Nd–Hf isotope results are presented in Table S1 and Table S2, respectively. The major and trace element compositions of the analyzed basalts overlap with previously reported data from the Hangai region (e.g., Barry et al. 2003; Hunt et al. 2012; Ancuta et al. 2018). The basalts possess variable SiO_2 from 44.6 to 53.0 wt% and total alkali (Na_2O + K_2O) from 5.1 to 8.2 wt%, and are thus classified mainly as alkali basalts including basanite, trachybasalt and basaltic trachyandesite (Fig. 4a). The CaO contents of the Jargalant basalts are highest among the Cenozoic basalts in central Mongolia and decrease together with MgO contents (Fig. 4b), while the CaO contents of other basalts keep constant irrespective of MgO contents. Basaltic samples from the Togo and Orkhon fields have FeO^T/MnO between 70 and 80, which are higher than those (FeO^T/MnO between 60 and 70) of basalts from the Tariat and Jargalant fields (Fig. 4c). For basalts from individual field, however, their FeO^T/MnO ratios remain invariant with falling MgO contents and are comparable to those of pyroxenite melts (e.g., Herzberg 2011).

As shown on the primitive mantle-normalized multi-element diagrams (Fig. 4d), all the basalts show OIB-like geochemical features, such as enrichments of Rb and Ba and positive Nb–Ta but negative Th–U anomalies (Hofmann and Jochum 1996). Their positive Nb–Ta anomalies are in contrast to the negative Nb–Ta anomalies of peridotite xenoliths from the Tariat basalts (Fig. 4d; Ionov et al. 1994). In addition, they all exhibit light REE (LREE)-enriched patterns (La/Sm = 3.3–6.1; La/Yb = 11.6–41.4) and positive Eu anomalies (δEu = 1.02–1.23). Their Nb/Ta ratios range from 17.1 to 20.4, which are similar to those of continental basalts but slightly higher than those of mid-ocean ridge basalts (MORB) and markedly higher than the estimate for continental crust (Münker et al. 2003; Pfänder et al. 2007).

The Tariat basalts possess relatively higher $^{87}Sr/^{86}Sr$, $^{143}Nd/^{144}Nd$, εNd and εHf values than those of other basalts (Fig. 5). Generally, the Sr–Nd isotopic compositions for the studied basalts are more enriched than the Hangai and Vitim mantle xenoliths (Stosch et al. 1986; Ionov et al. 1994, 1995), but less enriched than the Hangai crustal xenoliths (Barry et al. 2003). All the Hangai basalts fall between EM-1 and depleted mantle domains in terms of their Sr–Nd isotopes (Fig. 5a), and form a linear trend on the εNd–εHf diagram (Fig. 5b). Moreover, an Indian-type mantle source is favored as they show Indian MORB-like Nd and Hf isotopic compositions (Fig. 5b).

Olivine compositions

We analyzed the major element compositions of 476 olivine grains by EPMA, of which 286 high Fo (molecular Mg/(Mg+Fe)) grains were performed for trace element analysis by LA-ICP-MS. The analytical results are given in Table S3. There is no obviously compositional variations in relation with the ages of the host basalts. The analyzed olivines exhibit a wide range of Fo (71.2–91.8), which is correlated negatively with Ca (214–2573 ppm), Mn (774–3098 ppm), Li (1.2–9.0 ppm), Zn (42.5–276 ppm), Co (137–206 ppm) and Sc (2.0–5.8 ppm), and positively with Ni (316–3151 ppm) and Cr (41.6–331 ppm) (Figs. 6 and 7). No correlation is observed with V (2.8–10.6 ppm), Cu (0.38–9.5 ppm), Ti (10–345 ppm) and P (1.0–1356 ppm) (Fig. 7). In general, olivines of this study possess lower Ca and Mn but higher Ni concentrations than those crystallized from peridotite melts (Fig. 6; Herzberg 2011).

The relationships of olivine Fo contents with the whole-rock Mg# of their host basalts are illustrated in Figure 8. The Fe–Mg exchange partition coefficient between olivine and basaltic melt varies from 0.3 at 1 atm (Roeder and Emslie 1970) to 0.31–0.34 at 5–15 kbar (Ulmer 1989). Olivines from the Orkhon, Togo and Tariat basalts contain three populations including a Mg-rich group, an equilibrium group, and a Mg-depleted group, which plot respectively above, within and below the equilibrium field (Fig. 8). The Mg-rich olivine crystals are probably mantle xenocrysts given their extremely high Fo contents and low CaO contents (<0.1 wt.%; Figs. 6a and 6b), while the Mg-depleted olivine crystals probably crystallized from evolved and low-MgO melts. In contrast, olivines from the Jargalant basalts plot within and below the equilibrium field (Fig. 8).

DISCUSSION

Olivine phenocrysts or xenocrysts?

Olivine phenocrysts can be discriminated from mantle xenocrysts by means of their morphologic and compositional (e.g., Fo, Ca and Ti) differences. The minority of olivine grains in the Orkhon, Togo and Tariat basalts are characterized by angular to subround shapes and distinct core–rim textures with sawtooth edges (Fig. 3), implying that they are mantle xenocrysts (e.g., Kamenetsky et al. 2006). This inference is further supported by their high Fo values (up to 91.8) and low Ca (mostly < 600 ppm) and Ti (mostly < 70 ppm) contents in their cores (Figs. 6–8), as mantle olivines feature high Fo and low Ca (< 700 ppm) and Ti (< 70 ppm) (Sobolev et al. 2009; De Hoog et al. 2010; Foley et al. 2013). On the other hand, their rims exhibit decreasing Fo and Ni and increasing Mn and Ca, indicating that these xenocrysts experienced melt–rock interaction (Fig. 3). In contrast, the majority of olivine grains in the Orkhon, Togo and Tariat basalts are subhedral to euhedral in shape, and possess relatively low Fo (generally < 85) but high Ca (generally > 1000 ppm) and Ti (generally > 90 ppm) (Figs. 6–8), suggesting that they are magmatic phenocrysts. Additionally, these olivine phenocrysts are higher in Li, Zn, Co, Sc and P relative to the counterparts of olivine xenocrysts (Fig. 7). In the Jargalant basalts, all the olivines have Fo lower than 85,

This is the peer-reviewed, final accepted version for American Mineralogist, published by the Mineralogical Society of America.
The published version is subject to change. Cite as Authors (Year) Title. American Mineralogist, in press.
DOI: https://doi.org/10.2138/am-2020-7431. http://www.minsocam.org/

and Ti and Ca respectively higher than 70 and 1100 ppm, providing robust evidence for a magmatic origin.

Source lithology

While peridotite with modal olivine greater than 40% has long been regarded as the source lithology for basaltic melts (Kushiro and Kuno 1963), recent experimental studies suggest that partial melts of peridotite cannot match some key geochemical features of OIBs and continental alkaline basalts, including Al, Si, Ca and Ni contents (Hirose and Kushiro 1993; Hirschmann et al. 2003). As alternatives, other lithologies including hornblendite and pyroxenite have been proposed to be the possible sources for some alkaline basalts (Kogiso et al. 2003; Sobolev et al. 2007; Herzberg 2011). The contribution of hornblendite and pyroxenite versus that of peridotite can be discerned by comparing the bulk-rock and olivine compositions of basaltic magmas with high-pressure experimental products. High-pressure partial melts of hornblendite have TiO_2 > 3.5 wt% (Pilet et al. 2008), which are higher than those (1.9–3.1 wt%) of the Cenozoic basalts in central Mongolia, thus not favoring a hornblendite source. Moreover, given that partial melts of hornblendite have low contents (e.g., <100 ppm) of Cr and Ni (Rooney et al. 2017), the high Cr (125–463 ppm) and Ni (99–471 ppm) contents of the Cenozoic basalts in this study also argue against a hornblendite source. It has been demonstrated that pyroxenite melts have higher FeO/MnO, Zn/Mn and Zn/Fe×10^4 ratios than peridotite melts (50–60, 0.05 ± 0.006, 8.5 ± 0.9, respectively), as $K_D^{Fe/Mn}$, $K_D^{Zn/Mn}$ and $K_D^{Zn/Fe}$ are lower in pyroxenite relative to peridotite (Le

Roux et al. 2010; Herzberg 2011). However, cautions should be taken while using these ratios, because they will increase if fractionation of clinopyroxene/garnet occurs. For the Orkhon, Togo and Tariat basalts, their FeO/MnO, Zn/Mn and Zn/Fe ratios keep constant with falling MgO contents (Figs. 4c, 9a and 9b), indicating that these ratios were not affected by differentiation. Accordingly, their higher FeO/MnO, Zn/Mn and Zn/Fe ratios reflect a pyroxenite-rich source (Figs. 4c, 9a and 9b). In contrast, the Zn/Mn and Zn/Fe ratios of the Jargalant basalts increase with declining MgO contents (Figs. 9a and 9b), which, coupled with the positive correlation between CaO and MgO (Fig. 4b), suggest clinopyroxene fractionation. Hence, the above ratios of the Jargalant basalts are not applied to source discrimination. Moreover, pyroxenite melts have markedly lower Co/Fe$\times 10^4$ (<7) ratios than peridotite melts, as constrained by experimentally determined mineral/melt partition coefficients for Co and Fe (Davis et al. 2013). All of the basalts in this study have low Co/Fe$\times 10^4$ ratios (4.8–6.6), further implying that pyroxenite was an important component in the mantle sources of the Cenozoic basalts in central Mongolia.

Phenocrystic olivine normally crystallizes first in the primary basaltic melts, thus helping to identify source lithology. Given the lower bulk partition coefficient (*D*) for Ni but higher bulk *D* values for Ca and Mn in pyroxenite relative to peridotite, olivines crystallized from pyroxenite melts would possess higher Ni but lower Ca and Mn compared with the counterparts of peridotite melts (e.g., Sobolev et al. 2005, 2007; Herzberg 2011; Foley et al. 2013; Howarth and Harris 2017). As a whole, high-Fo (>82.5) olivines from each volcanic field have Ca and Mn lower than and Ni higher than olivines from peridotite melts, resembling olivines from the EI Hierro basanites that have been regarded to originate from a pyroxenite-rich source (Fig. 6; Gurenko et al. 2009). Furthermore, it is notable that even the high-Fo (>82.5) olivines of this study have Ni contents generally lower than olivines (Ni > 2500 ppm) from olivine-free pyroxenite melts (Herzberg 2011), reflecting an olivine-bearing rather than olivine-free pyroxenite source. Relative to the Orkhon and Togo olivines, the Tariat and Jargalant olivines possess lower Ni contents at a given Fo (Fig. 6f), therefore a relatively higher proportion of olivine is required in the pyroxenite source for the latter two. The amount of olivine in pyroxenite depends on the relative proportion of silicic melt versus mantle peridotite and a less proportion of silicic melt reacting with mantle peridotite is requested for olivine-bearing relative to olivine-free pyroxenite (Sobolev et al. 2005; Zhang et al. 2019). Moreover, it has been proposed that the Mn/Zn and 100*Mn/Fe ratios for olivine in equilibrium with pyroxenite melts (<13 and 1.05–1.35, respectively) are lower than those equilibrated with peridotite melts (>15 and >1.6, respectively) (Sobolev et al. 2007; Howarth and Harris 2017). In the case of Cenozoic basalts in central Mongolia, all of the olivines exhibit low Mn/Zn ratios (<13; Fig. 9c), supporting the presence of pyroxenite in the source. As shown in the 100*Mn/Fe versus 10000*Zn/Fe diagram (Fig. 9d), all the olivines from the Orkhon and Togo basalts have low 100*Mn/Fe ratios, consistent with a pyroxenite source; while most olivines from the Tariat and Jargalant basalts have low 100*Mn/Fe ratios and minor ones plot between the pyroxenite and peridotite ranges, indicating a lithologically-mixed source with dominant pyroxenite and subordinate peridotite.

DOI: https://doi.org/10.2138/am-2020-7431. http://www.minsocam.org/

Overall, it is concluded that olivine-bearing pyroxenite is the major source for the Cenozoic basalts in central Mongolia, while minor peridotite is involved in the source for the Jargalant and Tariat basalts.

Pyroxenite could exist either in the lithospheric or asthenospheric mantle. Here a lithospheric mantle origin is not favored, because peridotite xenoliths from the Hangai region are depleted in Nb–Ta which contrasts to the studied basalts (Fig. 4d) and they show more depleted Nd isotopes than the studied basalts (Fig. 5a; Stosch et al. 1986; Ionov et al. 1994). Pyroxenite in the asthenospheric mantle can be formed by direct transformation of subducted oceanic crust (stage I pyroxenite; Herzberg 2011) or by reaction between recycled continental/oceanic crust and its surrounding mantle peridotite via exhausting olivine and producing pyroxene (stage II pyroxenite; Sobolev et al. 2005; Mallik and Dasgupta 2012; Foley et al. 2013). Considering that the MgO contents of most Cenozoic basalts in this study are higher than those (MgO < 8.0 wt%; Pertermann and Hirschmann 2003) of melting products of silica-excess pyroxenite or bimineralic eclogite, it is inferred that stage I pyroxenite cannot be their direct source. Therefore, stage II pyroxenite is a more appropriate source. The olivines from the studied basalts have low Li contents (mostly < 5 ppm), which, together with the positive Nb–Ta anomalies and high Nb/Ta ratios of the whole rocks, demonstrates that continental crust components did not contribute to the stage II pyroxenite (Foley et al. 2013). Consequently, we suggest that recycled oceanic crust probably participated in the generation of stage II pyroxenite by reacting with its ambient peridotite, which is further confirmed by their trace element and isotope compositions.

DOI: https://doi.org/10.2138/am-2020-7431. http://www.minsocam.org/

Firstly, the negative Th–U and positive Ba anomalies (Fig. 4d) are compatible with the existence of recycled oceanic gabbro in the mantle source, as plagioclase has lower partition coefficients for Th and U relative to Ba (Hofmann and Jochum 1996). Secondly, the Nb/Ta ratios for the Orkhon (19.6 ± 0.55 (1σ)), Togo (19.5 ± 0.50 (1σ)), Tariat (18.5 ± 0.88 (1σ)) and Jargalant (18.8 ± 0.76 (1σ)) basalts are higher than that of upper asthenospheric mantle (e.g., MORB source; Pfänder et al. 2007), which can be ascribed to the involvement of partial melts of rutile-bearing eclogite in the mantle source. This is because rutile partitions Ta more strongly than Nb (i.e., $D_{Ta}^{rutile/melt} > D_{Nb}^{rutile/melt}$; Schmidt et al. 2004; Klemme et al. 2005). Thirdly, the Sr–Nd isotopic compositions of the Cenozoic basalts (Fig. 5a) indicate the involvement of EM1 component in the mantle source, which is generally regarded to be recycled oceanic crust components (Hofmann 1997).

Temperatures and oxygen fugacities of the magmas

The crystallization temperatures for phenocrystic olivines from the Cenozoic basalts in central Mongolia can be estimated using the olivine–liquid thermometer (Putirka 2008). Olivine compositions that fall within the Fe–Mg equilibrium fields are utilized, and the bulk-rock compositions are regarded as liquid compositions. The equation 22 of Putirka (2008) was used and yielded results of 1103–1321°C. The geothermometer of Lee et al. (2009) based on Fe–Mg exchange between olivine and melt can be used to estimate the mantle melting temperatures for basalts of this study. Considering the mineral assemblages and MgO variation diagrams, only samples without olivine xenocrysts and with MgO > 7.5 wt% are employed to minimize the effects of clinopyroxene fractionation and mantle olivine accumulation. Assuming a $K_D^{ol/melt}$(Fe/Mg) value of 0.32 and Fo of 90 for mantle olivine, the estimated melting temperatures range from 1343 to 1430°C, which are remarkably higher than the equilibrium temperatures (960 to 1090°C) of lithospheric mantle peridotites in the Hangai region (Fig. 10a; Harris et al. 2010).

It has been shown that V has several valence states (V^{2+}, V^{3+}, V^{4+} and V^{5+}) and $D_V^{ol/melt}$ is strongly dependent on the magma fugacity (fO_2) because V becomes more incompatible in silicate minerals under conditions of high fO_2 where V^{5+} is common (Canil 1997; Canil and Fedortchouk 2001). Based on the $D_V^{ol/melt}$ oxybarometer of Canil and Fedortchouk (2001) and V contents in olivines (Fo = 83–85) and equilibrated hosts, the fO_2 has been estimated to be +0.42 (± 0.18, 1σ, n = 59), +0.28 (± 0.16, 1σ, n = 28), –0.26 (± 0.1, 1σ, n = 16) and –0.08 (± 0.12, 1σ, n = 24) log units relative to the FMQ (fayalite–magnetite–quartz) buffer for the Orkhon, Togo, Tariat and Jargalant basalts, respectively (Fig. 10b). There exists a negative correlation between calculated fO_2 and olivine Mn/Zn among the samples (Fig. 10b), which probably suggests that the high fO_2 but low Mn/Zn basalts (i.e., Orkhon and Togo) involved more proportions of recycled, oxidized materials (e.g., pyroxenite) in their mantle sources (Brounce et al. 2017). This explanation is consistent with the lower Mn/Zn and 100*Mn/Fe ratios of the Orkhon and Togo olivines compared to those of the Tariat and Jargalant olivines (Figs. 9c and 9d).

Initiation of the Cenozoic basalts in central Mongolia

The mechanism regarding the initiation of the Cenozoic basalts in central Mongolia is not well known yet, and variable geodynamic models have been proposed including mantle plume (Windley and Allen 1993; Yarmolyuk et al. 2015), Pacific subudction (Meng et al. 2018), lithospheric delamination (Hunt et al. 2012) and India–Eurasia collision (Cunningham 2001). Based on our new geochemical data and previously published data, these models can now be evaluated. Given that there is no geophysical evidence for a deep mantle upwelling and no plume-related metallogenesis or flood basalts, a deep mantle plume is not evident beneath the Hangai region (Bryan and Ernst 2008). Moreover, Barry et al. (2007) reported He isotopic data for olivines separated from basalts and mantle xenoliths in the Hangai volcanic province, and their $^{3}He/^{4}He$ ratios are similar to those of MORB, indicating a shallow asthenospheric rather than a lower primordial mantle. Importantly, the estimated mantle melting temperatures (1343–1430°C) that are slightly higher than the corresponding potential temperatures fall within the range of upper mantle potential temperature (1350 ± 50°C; Herzberg and Gazel 2009), but are lower than the potential temperature for large igneous provinces (e.g., 1510–1640°C for Deccan Traps). This observation provides robust evidence for an upper mantle source, thus a deep mantle plume is not favored.

It has been geophysically demonstrated that subducted Pacific slab tends to be subhorizontal and stagnant within the mantle transition zone (410–660 km) beneath the east Asian continent (Zhao 2004), and its western end does not go beyond the

NNE-trending Daxing'anling–Taihangshan Gravity Lineament (DTGL; Xu 2007). It is likely that Cenozoic basalts in the east Asia were triggered by the subduction of the Pacific slab as well as concurrent fluids/melts released from the stagnant Pacific slab (Kuritani et al. 2011; Wang et al. 2015). Nevertheless, the Hangai volcanic province is 1500 to 2000 km away from the DTGL, which seems too far to be affected by the stagnant Pacific slab. Moreover, the calculated fO_2 values (ΔFMQ –0.26 to +0.42) for the studied Cenozoic basalts are comparable to those of MORB (ΔFMQ –0.41 to +0.56; Cottrell and Kelley 2011) but are lower than those of back-arc basalts (ΔFMQ +1.0 to +1.5) and arc island basalts (ΔFMQ +1.4 to +2.7) (Kelley and Cottrell 2009). The above comparisons indicate that these Cenozoic basaltic magmas are much less oxidized than arc magmas, thus not supporting the connection with the stagnant Pacific slab.

Delamination refers to the sinking of the lower crust and lithospheric mantle into the asthenosphere, which is mainly driven by the negative buoyancy of lower continental lithosphere due to the eclogite phase transition (Schott and Schmeling 1998). However, the lower-crust xenoliths in the Hangai region are mainly granulites, which have been explained to be formed by basaltic underplating at the crust–mantle boundary (Stosch et al. 1995). Besides, based on the geophysical–petrological inversion, the density of mid-lower crust in the Hangai region is estimated to be 3.16–3.20 g/cm^3 (Fullea et al. 2012), which is lower than eclogite (3.4–3.8 g/cm^3; Lustrino 2005) and upper mantle (~3.3 g/cm^3), implying that lithospheric delamination is limited, if any. As an alternative, convective removal of the lower-most lithosphere induced by upwelling asthenosphere may serve as the trigger of Cenozoic basalts in the Hangai region. This inference is supported by the relatively thin thickness for lithospheric mantle (<55 km) in the Hangai region (Barruol et al. 2008; Fullea et al. 2012). In this scenario, upwelling asthenosphere will heat and soften the lower-most mantle lithosphere, and subsequently the softened part is inclined to be mechanically removed (Davies 1994). Meanwhile, the upwelling asthenosphere will partially melt and the resultant melts may assimilate the overlying mantle lithosphere, as evidenced by the existence of olivine xenocrysts, which finally generated the studied basalts (Fig. 11). In fact, a slightly warmer asthenospheric upwelling from the transition zone has been detected by Chen et al. (2015) using the adjoint tomography technique. On the other hand, asthenospheric upwelling could result from shear flow in the upper mantle, produced by the motion of the overlying plate relative to the convecting mantle. In central Mongolia, GPS and SKS both depict that the lithosphere escapes toward the east within a transpressive tectonic regime (Barruol et al. 2008), probably as a response to the north–south shortening by India–Eurasia collision, which would introduce a shear flow in the underlying mantle. In addition, seismic tomography and numerical simulation indicate that the collision between India and Eurasia could have driven significant lateral extrusion of asthenospheric mantle under the Asian continent, which may lead to diffuse asthenospheric upwelling (Liu et al. 2004). Collectively, we propose that the far-field effect of India–Eurasia convergence plays a major role in tapping the upper asthenosphere mantle, subsequent melting of which give rise to the pervasive Cenozoic basalts in the Hangai region.

Trigger of Cenozoic uplift in the Hangai Mountains

The Hangai Mountains embedded in the Mongolian Plateau (~2000 m elevation in average) locally reach elevation of 4000 m and are characterized by low-relief and long-wavelength topography. Understanding the uplift process of this mountain range is critical to decipher its role in creating the arid climate of northern Gobi in central Asia (West et al. 2013; Caves et al. 2014). On the basis of apatite (U-Th)/He thermochronometer, the bedrock apatite samples yielded single-grain ages from ~70 to 200 Ma with a mean of 123 ± 24 Ma and the detrital ones gave age populations of ~115 to 130 Ma, indicating that the Hangai Mountains were mainly uplifted in the Cretaceous (McDannell et al. 2018). Such uplift was probably driven by collision-related tectonism followed by the Jurassic–Cretaceous closure of the Mongol–Okhotsk Ocean (Van der Voo et al. 2015; McDannell et al. 2018). In addition to the Cretaceous uplift, modest uplift in the mid–late Cenozoic has been suggested based on some recent work. For instance, the $\delta^{13}C$ values of paleosol carbonates in central Mongolia increase in the Oligocene, which have been attributed to dynamic increase in aridity induced by regional surface uplift (Caves et al. 2014). Additionally, analyses of size distributions of vesicles at the tops and bottoms of basaltic lava flows imply that the Hangai Mountains experienced uplift of ~1 km during the past 9 Myrs (Sahagian et al. 2016). Nevertheless, the mechanism behind the Cenozoic uplift remains unclear, although several models already existed, such as localized mantle plume activity, lithospheric delamination, underplated mafic cumulates and asthenosphere upwelling (Windley and Allen 1993; Petit et al. 2002, Hunt et al. 2012; Chen et al. 2015). As discussed above, deep mantle plume and lithospheric delamination are not evident in the Hangai region, thus these two models seem unlikely. Underplated mafic cumulates and dynamic support from asthenosphere upwelling may have contributed to the Cenozoic uplift of the Hangai Mountains (Petit et al. 2002; Chen et al. 2015), but we here emphasize the importance of convective removal of the lower-most lithosphere through asthenosphere–lithosphere interaction based on our newly obtained data (e.g., Molnar et al. 1993).

Upwelling asthenosphere may not only cause mechanical erosion of the mantle lithosphere but also chemically react with it. In the process of mechanical erosion, the lower-most mantle lithosphere will be heated by upwelling asthenosphere and consequently the weakened and softened parts will be removed by horizontal asthenosphere flow (Davies 1994). This is supported by the Bouguer gravity anomaly (i.e., a large, negative (–300 mGal) and long-wavelength anomaly) beneath the Hangai Mountains that argues for a lithospheric thinning (Tiberi et al. 2008). In turn, the mass deficit in the lithosphere could provide an isostatic contribution to the Hangai surface uplift. On the other hand, melt–rock interaction has occurred as evidenced by the zoned textures in olivine xenocrysts (Fig. 3). When mantle olivine xenocrysts are trapped in basaltic melts, reaction between the two (e.g., Fe–Mg exchange) could occur due to the thermal and compositional disequilibria (Kelemen et al. 1990). Generally, basaltic melt is enriched in Fe, Mn and Ca but poor in Mg and Ni relative to the mantle peridotite, therefore reaction will cause the mantle olivines to evolve towards Fe, Mn and Ca enrichment but Mg and Ni depletion, namely the low-Fo olivines, which is the case of this study (Fig. 3). Preservation of zoned mantle olivine xenocrysts owing to rapid magma ascent may reflect that melt–rock reaction was widespread in the mantle lithosphere. Moreover, the texture of spongy olivine rimming orthopyroxene has been found in the peridotite xenoliths from the Hangai region, further suggesting the chemical interaction between mantle orthopyroxenes and basaltic melts (Harris et al. 2010). Such reactions would change both the chemical compositions within mineral phases (e.g., transformation of high-Mg# to low-Mg# peridotites) and the proportions of mineral phases in mantle peridotites (e.g., increasing orthopyroxene contents), which can modify the rheology of the mechanical boundary layer and accelerate the mechanical erosion (e.g., Dijkstra et al. 2002; Zhu et al. 2009). Accordingly, we propose that the combined chemical modification and mechanical erosion of the mantle lithosphere induced by upwelling asthenosphere could have caused the Cenozoic isostatic uplift of the Hangai Mountains (Fig. 11).

IMPLICATIONS

The Cenozoic basalts in central Mongolia have higher Fe/Mn, Zn/Mn and Zn/Fe ratios than peridotitic melts, which, coupled with the phenocrystic olivines possessing lower Ca, Mn, Mn/Zn and Mn/Fe but higher Ni relative to those of peridotitic melts, demonstrates a pyroxenite-rich source. We propose that secondary pyroxenite was created by the reaction of recycled oceanic crust with its surrounding peridotite, based on their negative Th–U anomalies, high Nb/Ta ratios and EM1-like Sr–Nd–Hf isotopic compositions. In combination with previously published data, the estimated mantle melting temperatures (1343–1430°C) and magma oxygen fugacities (ΔFMQ –0.26 to +0.42) do not favor the connection with a deep mantle plume or the stagnant Pacific slab. Conversely, the far-field effect of India–Eurasia collision may account for the upwelling of upper asthenospheric mantle, subsequent melting of which gave rise to the dispersive Cenozoic volcanism. On the other hand, the zoned mantle olivine xenocrysts reflect that melt–rock reaction was widespread in the mantle lithosphere, which may change the rheology and accelerate the mechanical erosion of mantle lithosphere. As a consequence, mass deficit in the lithosphere could have caused the Cenozoic isostatic uplift in the Hangai region.

ACKNOWLEDGEMENTS

We thank Le Zhang, Jinlong Ma, Changming Xing, Dan Wu and Xiao Fu for their help with the geochemical analyses, and Xiaobo Xu and Yafeng Yu for the field assistance. We appreciate Associate Editor Calvin Barnes for his kind editorial help and constructive comments. We are grateful to two anonymous reviewers, whose insightful and constructive reviews greatly improve this manuscript. This work was financially supported by the Strategic Priority Research Program of the Chinese Academy of Sciences (Grant No. XDB18000000), the CPSF–CAS Joint Foundation for Excellent Postdoctoral Fellows (2017LH019), the International Partnership Program of CAS (Grant No. 132744KYSB20190039), the National Science Foundation of China (41603030, 41973021), and the Hong Kong RGC research projects (17303415, 17302317). This is a contribution of the Chemical Geodynamic Joint Laboratory between HKU and GIG, CAS.

REFERENCES CITED

Ancuta, L.D., Zeitler, P.K., Idleman, B.D., and Jordan, B.T. (2018) Whole-rock $^{40}Ar/^{39}Ar$ geochronology, geochemistry, and stratigraphy of intraplate Cenozoic volcanic rocks, central Mongolia. Geological Society of America Bulletin, 130, 1397–1408.

Badarch, G., Cunningham, W.D., and Windley, B.F. (2002) A new terrane subdivision for Mongolia: Implications for the Phanerozoic crustal growth of central Asia. Journal of Asian Earth Sciences, 21, 87–110.

Barruol, G., Deschamps, A., Déverchère, J., Mordvinova, V.V., Ulziibat, M., Perrot, J., Artemiev, A.A., Dugarmaa, T., and Bokelmann, G.H.R. (2008) Upper mantle flow beneath and around the Hangay dome, Central Mongolia. Earth and Planetary Science Letters, 274, 221–233.

Barry, T.L., Ivanov, A., Rasskazov, S.V., Demonterova, E.I., Dunai, T.J., Davies, G.R., and Harrison, D. (2007) Helium isotopes provide no evidence for deep mantle involvement in widespread Cenozoic volcanism across Central Asia. Lithos, 95, 415–424.

Barry, T.L., Saunders, A.D., Kempton, P.D., Windley, B.F., Pringle, M.S., Dorjnamjaa, D., and Saandar, S. (2003) Petrogenesis of Cenozoic basalts from Mongolia: Evidence for the role of asthenospheric versus metasomatized lithospheric mantle sources. Journal of Petrology, 44, 55–91.

Braun, J. (2010) The many surface expressions of mantle dynamics. Nature Geoscience, 3, 825–833.

Brounce, M., Stolper, E., and Eiler, J. (2017) Redox variations in Mauna Kea lavas, the oxygen fugacity of the Hawaiian plume, and the role of volcanic gases in Earth's oxygenation. Proceedings of the National Academy of Sciences, 114, 8997–9002.

Bryan, S.E., and Ernst, R.E. (2008) Revised definition of Large Igneous Provinces (LIPs). Earth-Science Reviews, 86, 175–202.

Canil, D. (1997) Vanadium partitioning and the oxidation state of Archaean komatiites magmas.

Nature, 389, 842–845.

Canil, D., and Fedortchouk, Y. (2001) Olivine–liquid partitioning of vanadium and other trace elements, with applications to modern and ancient picrites. Canadian Mineralogist, 39, 319–330.

Caves, J.K., Sjostrom, D.J., Mix, H.T., Winnick, M.J., and Chamberlain, C.P. (2014) Aridification of central Asia and uplift of the Altai and Hangay mountains, Mongolia: Stable isotope evidence. American Journal of Science, 314, 1171–1201.

Chauvel, C., Lewin, E., Carpentier, M., Arndt, N.T., and Marini, J.C. (2008) Role of recycled oceanic basalt and sediment in generating the Hf–Nd mantle array. Nature Geoscience, 1, 64–67.

Chen, M., Niu, F.L, Liu, Q.Y., and Tromp, J. (2015) Mantle-driven uplift of Hangai Dome: New seismic constraints from adjoint tomography. Geophysical Research Letters, 42, 6967–6974.

Cottrell, E., and Kelley, K.A. (2011) The oxidation state of Fe in MORB glasses and the oxygen fugacity of the upper mantle. Earth and Planetary Science Letters, 305, 270–282.

Cunningham, W.D. (2001) Cenozoic normal faulting and regional doming in the southern Hangay region, Central Mongolia: implications for the origin of the Baikal rift province. Tectonophysics, 331, 389–411.

Davies, G.F. (1994) Thermomechanical erosion of the lithosphere by mantle plumes. Journal of Geophysical Research: Solid Earth, 99, 15709–15722.

Davis, F.A., Humayun, M., Hirschmann, M.M., and Cooper, R.S. (2013) Experimentally determined mineral/melt partitioning of first-row transition elements (FRTE) during partial melting of peridotite at 3 GPa. Geochimica et Cosmochimica Acta, 104, 232–260.

De Hoog, J.C.M., Gall, L., and Cornell, D.H. (2010) Trace-element geochemistry of mantle olivine and application to mantle petrogenesis and geothermobarometry. Chemical Geology, 270, 196–215.

Dijkstra, A.H., Drury, M.R., Vissers, R.L.M., and Newman, J. (2002) On the role of melt-rock reaction in mantle shear zone formation in the Othris Peridotite Massif (Greece). Journal of Structural Geology, 24, 1431–1450.

Elburg, M., Vroon, P., van der Wagt, B., and Tchalikian, A. (2005) Sr and Pb isotopic composition of five USGS glasses (BHVO-2G, BIR-1G, BCR-2G, TB-1G, NKT-1G).

Chemical Geology, 223, 196–207.

Foley, S.F., Prelevic, D., Rehfeldt, T., and Jacob, D.E. (2013) Minor and trace elements in olivines as probes into early igneous and mantle melting process. Earth and Planetary Science Letters, 363, 181–191.

Fullea, J., Lebedev, S., Agius, M.R., Jones, A.G., and Afonso, J.C. (2012) Lithospheric structure in the Baikal–central Mongolia region from integrated geophysical-petrological inversion of surface-wave data and topographic elevation. Geochemistry Geophysics Geosystems, 13, Q0AK09.

Gurenko, A.A., Sobolev, A.V., Hoernle, K.A., Hauff, F., and Schmincke, H.U. (2009) Enriched, HIMU–type peridotite and depleted recycled pyroxenite in the Canary plume: a mixed-up mantle. Earth and Planetary Science Letters, 277, 514–524.

Harris, N., Hunt, A., Parkinson, I., Tindle, A., Uondon, M., and Hammond, S. (2010) Tectonic implications of garnet-bearing mantle xenoliths exhumed by Quaternary magmatism in the Hangai Dome, central Mongolia. Contributions to Mineralogy and Petrology, 160, 67–81.

Herzberg, C.T. (1978) Pyroxene geothermometry and geobarometry: experimental and thermodynamic evaluation of some subsolidus phase relations involving pyroxenes in the system CaO-MgO-Al_2O_3-SiO_2. Geochimica et Cosmochimica Acta, 42, 945–957.

Herzberg, C., and Asimow, P.D. (2008) Petrology of some oceanic island basalts: PRIMELT2.XLS software for primary magma calculation. Geochemistry Geophysics Geosystems, 8, Q09001.

Herzberg, C., and Gazel, E. (2009) Petrological evidence for secular cooling in mantle plumes. Nature, 458, 619–622.

Herzberg, C. (2011) Identification of source lithology in the Hawaiian and Canary Islands: implications for origin. Journal of Petrology, 52, 113–146.

Hirose, K., and Kushiro, I. (1993) Partial melting of dry peridotites at high pressures: Determination of compositions of melts segregated from peridotite using aggregates of diamond. Earth and Planetary Science Letters, 114, 477–489.

Hirschmann, M.M., Kogiso, T., Baker, M.B., and Stolper, E.M. (2003) Alkalic magmas generated by partial melting of garnet pyroxenite. Geology, 31, 481–484.

Hofmann, A.W., and Jochum, K.P. (1996) Source characteristics derived from very incompatible

DOI: https://doi.org/10.2138/am-2020-7431. http://www.minsocam.org/

trace elements in Mauna Loa and Mauna Kea basalts, Hawaii Scientific Drilling Project. Journal of Geophysical Research: Solid Earth, 101, 11831–11839.

Hofmann, A.W. (1997) Mantle geochemistry: the message from oceanic volcanism. Nature, 385, 219–229.

Howarth, G.H., and Harris, C. (2017) Discriminating between pyroxenite and peridotite sources for continental flood basalts (CFB) in southern Africa using olivine chemistry. Earth and Planetary Science Letters, 475, 143–151.

Hunt, A.C., Parkinson, I.J., Harris, N.B.W., Barry, T.L., Rogers, N.W., and Yondon. M. (2012) Cenozoic volcanism on the Hangai dome, Central Mongolia: Geochemical evidence for changing melt sources and implications for mechanisms of melting. Journal of Petrology, 53, 1913–1942.

Ionov, D.A., Hofmann, A.W., and Shimizu, N. (1994) Metasomatism-induced melting in mantle xenoliths from Mongolia. Journal of Petrology, 35, 753–785.

Ionov, D.A., O'Reilly, S.Y., and Ashchepkov, I.V. (1995) Feldspar-bearing lherzolite xenoliths in alkali basalts from Hamar-Daban, southern Baikal region, Russia. Contributions to Mineralogy and Petrology, 122, 174–190.

Ionov, D. (2002) Mantle structure and rifting processes in the Baikal–Mongolia region: geophysical data and evidence from xenoliths in volcanic rocks. Tectonophysics, 351, 41–60.

Ivanov, A.V., Demonterova, E.I., He, H.Y., Perepelov, A.B., Travin, A.V., and Lebedev, V.A. (2015) Volcanism in the Baikal rift: 40 years of active-versus-passive model discussion. Earth-Science Reviews, 148, 18–43.

Johnson, J.S., Gibson, S.A., Thompson, R.N., and Nowell, G.M. (2005) Volcanism in the Vitim volcanic field, Siberia: Geochemical evidence for a mantle plume beneath the Baikal rift zone. Journal of Petrology, 46, 1309–1344.

Kamenetsky, V.S., Elburg, M., Arculus, R., and Thomas, R. (2006) Magmatic origin of low-Ca olivine in subduction-related magmas: Co-existence of contrasting magmas. Chemical Geology, 233, 346–357.

Katz, R.F., Spiegelman, M., and Langmuir, C.H. (2003) A new parameterization of hydrous mantle melting. Geochemistry Geophysics Geosystems, 4, 1073.

Kelemen, P.B., Joyce, D.B., Webster, J.D., and Holloway, J.R. (1990) Reaction between ultramafic rock and fractionating basaltic magma II. Experimental investigation of reaction between olivine tholeiite and harzburgite at 1150–1050°C and 5kb. Journal of Petrology, 31, 99–134.

Klemme, S., Prowatke, S., Hametner, K., and Günther, D. (2005) Partitioning of trace elements between rutile and silicate melts: Implications for subduction zones. Geochimica et Cosmochimica Acta, 69, 2361–2371.

Kelley, K.A., and Cottrell, E. (2009) Water and the oxidation state of subduction zone magmas. Science, 325, 605–607.

Kogiso, T., Hirschmann, M.M., and Frost, D.J. (2003) High pressure partial melting of garnet pyroxenite: possible mafic lithologies in the source of ocean island basalts. Earth and Planetary Science Letters, 216, 603–617.

Kuritani, T., Ohtani, E., and Kimura, J.I. (2011) Intensive hydration of the mantle transition zone beneath China caused by slab stagnation. Nature Geoscience, 4, 713–716.

Kushiro, I., and Kuno, H. (1963) Origin of primary basalt magmas and classification of basaltic rocks. Journal of Petrology, 4, 75–89.

Lambart, S., Baker, M.B., and Stolper, E.M. (2016) The role of pyroxenite in basalt genesis: Melt-PX, a melting parameterization for mantle pyroxenites between 0.9 and 5 GPa. Journal of Geophysical Research: Solid Earth, 121, 5708–5735.

Le Bas, M.J., Le Maitre, R.W., Strekeisen, A., and Zanettin, B. (1986) Chemical classification of volcanic rocks based on the total alkali–silica diagram. Journal of Petrology, 27, 745–750.

Lee, C.T.A., Luffi, P., Plank, T., Dalton, H., and Leeman, W.P. (2009) Constraints on the depths and temperatures of basaltic magma generation on Earth and other terrestrial planets using new thermobarometers for mafic magmas. Earth and Planetary Science Letters, 279, 20–33.

Le Roux, V., Lee, C.T.A., and Turner, S.J. (2010) Zn/Fe systematics in mafic and ultramafic systems: implications for detecting major element heterogeneities in the Earth's mantle. Geochimica et Cosmochimica Acta, 74, 2779–2796.

Li, X.C., and Zhou, M.F. (2018) The nature and origin of hydrothermal REE mineralization in the Sin Quyen deposit, northwestern Vietnam. Economic Geology, 113, 645–673.

Li, X.H., Li, Z.X., Wingate, M.T.D., Chung, S.L., Liu, Y., Lin, G.C., and Li, W.X. (2006) Geochemistry of the 755 Ma Mundine Well dyke swarm, northwestern Australia: Part of a

Neoproterozoic mantle superplume beneath Rodinia?. Precambrian Research, 146, 1–15.

Liu, M., Cui, X. J., and Liu, F.T. (2004) Cenozoic rifting and volcanism in eastern China: a mantle dynamic link to the Indo–Asian collision?. Tectonophysics, 393, 29–42.

Liu, Y.S., Hu, Z.C., Gao, S., Günther, D., Xu, J., Gao, C.G., and Chen, H.H. (2008) In situ analysis of major and trace elements of anhydrous minerals by LA-ICP-MS without applying an internal standard. Chemical Geology, 257, 34–43.

Lustrino, M. (2005) How the delamination and detachment of lower crust can influence basaltic magmatism. Earth-Science Reviews, 72, 21–38.

Mallik, A., and Dasgupta, R. (2012) Reaction between MORB–eclogite derived melts and fertile peridotite and generation of ocean island basalts. Earth and Planetary Science Letters, 329–330, 97–108.

McDannell, K.T., Zeitler, P.K. and Idleman, B.D. (2018) Relict topography within the Hangay Mountains in central Mongolia: Quantifying long-term exhumation and relief change in an old landscape. Tectonics, 37, 2531–2558.

Meng, F.C., Safonova, I., Chen, S.S., and Rioual, P. (2018) Late Cenozoic intra-plate basalts of the Greater Khingan Range in NE China and Khangai Province in Central Mongolia. Gondwana Research, 63, 65–84.

Molnar, P., England, P., and Martinod, J. (1993) Mantle dynamics, uplift of the Tibetan Plateau, and the Indian monsoon. Reviews of Geophysics, 31, 357–396.

Münker, C., Pfänder, J.A., Weyer, S., Büchl, A., Kleine, T., and Mezger, K. (2003) Evolution of planetary cores and the Earth–Moon system from Nb/Ta systematics. Science, 301, 84–87.

O'Neill, H.S.C. (1981) The transition between spinel lherzolite and garnet lherzolite, and its use as a geobarometry. Contributions to Mineralogy and Petrology, 77, 185–194.

Pearce, J.A., Kempton, P.D., Nowell, G.M., and Noble, S.R. (1999) Hf-Nd element and isotope perspective on the nature and provenance of mantle and subduction components in Western Pacific arc-basin systems. Journal of Petrology, 40, 1579–1611.

Pertermann, M., and Hirschmann, M.M. (2003) Anhydrous partial melting experiments on MORB-like eclogite: Phase relations, phase compositions and mineral-melt partitioning of major elements at 2–3 GPa. Journal of Petrology, 44, 2173–2201.

Petit, C., Déverchère, J., Calais, E., San'kov, V., and Fairhead, D. (2002) Deep structure and mechanical behavior of the lithosphere in the Hangai–Hövsgöl region, Mongolia: new constraints from gravity modeling. Earth and Planetary Science Letters, 197, 133–149.

Pfänder, J.A., Münker, C., Stracke, A., and Mezger, K. (2007) Nb/Ta and Zr/Hf in ocean island basalts—implications for crust–mantle differentiation and the fate of Niobium. Earth and Planetary Science Letters, 254, 158–172.

Pilet, S., Baker, M.B., and Stolper, E.M. (2008) Metasomatized lithosphere and the origin of alkaline lavas. Science, 320, 916–919.

Putirka, K.D. (2008) Thermometers and barometers for volcanic systems. Reviews in Mineralogy and Geochemistry, 69, 61–120.

Putirka, K., Ryerson, F.J., Perfit, M., and Ridley, W.I. (2011) Mineralogy and composition of the Oceanic Mantle. Journal of Petrology, 52, 279–313.

Roeder, P., and Emslie, R.F. (1970) Olivine–liquid equilibrium. Contributions to Mineralogy and Petrology, 29, 275–289.

Rooney, T.O., Nelson, W.R., Ayalew, D., Hanan, B., Yirgu, G., and Kappelman, J. (2017) Melting the lithosphere: Metasomes as a source for mantle-derived magmas. Earth and Planetary Science Letters, 461, 105–118.

Sahagian, D., Proussevitch, A., Ancuta, L.D., Idleman, B.D., and Zeitler, P.K. (2016) Uplift of central Mongolia recorded in vesicular basalts. The Journal of Geology, 124, 435–445.

Savatenkov, V.M., Yarmolyuk, V.V., Kudryashova, E.A., and Kozlovskii, A.M. (2010) Sources and geodynamics of the Late Cenozoic volcanism of Central Mongolia: Evidence from isotope-geochemical studies. Petrology, 18, 278–307.

Schmidt, M.W., Dardon, A., Chazot, G., and Vannucci, R. (2004) The dependence of Nb and Ta rutile–melt partitioning on melt composition and Nb/Ta fractionation during subduction processes. Earth and Planetary Science Letters, 226, 415–432.

Schott, B., and Schmeling, H. (1998) Delamination and detachment of a lithospheric root. Tectonophysics, 296, 225–247.

Smith, S.G., Wegmann, K.W., Ancuta, L.D., Gosse, J.C., and Hopkins, C.E. (2016) Paleotopography and erosion rates in the central Hangay Dome, Mongolia: Landscape evolution since the mid-Miocene. Journal of Asian Earth Sciences, 125, 37–57.

Sobolev, A.V., Hofmann, A.W., Sobolev, S.V., and Nikogosian, I.K. (2005) An olivine-free

DOI: https://doi.org/10.2138/am-2020-7431. http://www.minsocam.org/

mantle source of Hawaiian shield basalts. Nature, 434, 590–597.

Sobolev, A.V., Hofmann, A.W., Kuzmin, A.V., Yaxley, G.M., Arndt, N.T., Chung, S.L., Danyushevsky, L.V., Elliott, T., Frey, F.A., Garcia, M.O., Gurenko, A.A., Kamenetsky, V.S., Kerr, A.C., Krivolutskaya, N.A., Matvienkov, V.V., Nikogosian, I.K., Rocholl, A., Sigurdsson, I.A., Sushchevskaya, N.M., and Teklay, M. (2007) The amount of recycled crust in sources of mantle-derived melts. Science, 316, 412–417.

Sobolev, N.V., Logvinova, A.M., Zedgenizov, D.A., Pokhilenko, N.P., Malygina, E.V., Kuzmin, D.V., and Sobolev, A.V. (2009) Petrogenetic significance of minor elements in olivines from diamonds and peridotite xenoliths from kimberlites of Yakutia. Lithos, 112S, 701–713.

Stosch, H.G., Lugmair, G.W., and Kovalenko, V.I. (1986) Spinel peridotite xenoliths from the Tariat Depression, Mongolia. II: Geochemistry and Nd and Sr isotopic composition and their implications for the evolution of the subcontinental lithosphere. Geochimica et Cosmochimica Acta, 50, 2601–2614.

Stosch, H.G., Ionov, D.A., Puchtel, I.S., Galer, S.J.G., and Sharpouri, A. (1995) Lower crustal xenoliths from Mongolia and their bearing on the nature of the deep crust beneath central Asia. Lithos, 36, 227–242.

Sun, S.S., and McDonough, W.F. (1989) Chemical and isotopic systematics of oceanic basalts: Implications for mantle composition and processes. Geological Society London Special Publications, 42, 313–345.

Tanaka, T., Togashi, S., Kamioka, H., Amakawa, H., Kagami, H., Hamamoto, T., Yuhara, M., Orihashi, Y., Yoneda, S., Shimizu, H., Kunimaru, T., Takahashi, K., Yanagi, T., Nakano, T., Fujimaki, H., Shinjo, R., Asahara, Y., Tanimizu, M., and Dragusanu, C. (2000) JNdi-1: a neodymium isotopic reference in consistency with LaJolla neodymium. Chemical Geology, 168, 279–281.

Tiberi, C., Deschamps, A., Déverchère, J., Petit, C., Perrot, J., Appriou, D., Mordvinova, V., Dugaarma, T., Ulzibaat, M., and Artemiev, A.A. (2008) Asthenospheric imprints on the lithosphere in Central Mongolia and Southern Siberia from a joint inversion of gravity and seismology (MOBAL experiment). Geophysical Journal International, 175, 1283–1297.

Tollan, P.M.E., O'Neill, H.S.C., Hermann, J., Benedictus, A., and Arculus, R.J. (2015) Frozen melt–rock reaction in a peridotite xenolith from sub-arc mantle recorded by diffusion of trace elements and water in olivine. Earth and Planetary Science Letters, 422, 169–181.

Ulmer, P. (1989) The dependence of Fe^{2+}–Mg cation-partitioning between olivine and basaltic liquid on pressure, temperature and composition. Contributions to Mineralogy and Petrology, 101, 261–273.

Van der Voo, R., van Hinsbergen, D.J.J., Domeier, M., Spakman, W., and Torsvik, T.H. (2015) Latest Jurassic-earliest Cretaceous closure of the Mongol-Okhotsk Ocean: A paleomagnetic and seismological-tomographic analysis. Geological Society of America Special Papers, 513, 589–606.

Vassallo, R., Jolivet, M., Ritz, J.F., Braucher, R., Larroque, C., Sue, C., Todbileg, M., and Javkhlanbold, D. (2007) Uplift age and rates of the Gurvan Bogd system (Gobi-Altay) by apatite fission track analysis. Earth and Planetary Science Letters, 259, 333–346.

Walker, R.T., Nissen, E., Molor, E., and Bayasgalan, A. (2007) Reinterpretation of the active faulting in central Mongolia. Geology, 35, 759–762.

Wang, X.C., Wilde, S.A., Li, Q.L., and Yang, Y.N. (2015) Continental flood basalts derived from the hydrous mantle transition zone. Nature Communications, 6, 7700.

Wei, G.J., Liang, X.R., Li, X.H., and Liu, Y. (2002) Precise measurement of Sr isotopic composition of liquid and solid base using (LP) MC-ICPMS. Geochimica, 31, 295–299.

West, A.J., Fox, M., Walker, R.T., Carter, A., Harris, T., Watts, A.B., and Gantulga, B. (2013) Links between climate, erosion, uplift, and topography during intracontinental mountain building of the Hangay Dome, Mongolia. Geochemistry, Geophysics, Geosystems, 14, 5171–5193.

Windley, B.F., and Allen, M.B. (1993) Mongolian plateau: Evidence for a late Cenozoic mantle plume under central Asia. Geology, 21, 295–298.

Wu, F.Y., Li, X.H., Zheng, Y.F., and Gao, S. (2007) Lu-Hf isotopic systematics and their applications in petrology. Acta Petrologica Sinica, 23, 185–220.

Xing, C.M., Wang, C.Y., and Tan, W. (2017) Disequilibrium growth of olivine in mafic magmas revealed by phosphorus zoning patterns of olivine from mafic–ultramafic intrusions. Earth and Planetary Science Letters, 479, 108–119.

Xu, Y.G. (2007) Diachronous lithospheric thinning of the North China Craton and formation of the Daxin'anling-Taihangshan gravity lineament. Lithos, 96, 281–298.

Yarmolyuk, V.V., Kudryashova, E.A., Kozlovsky, A.M., Lebedev, V.A., and Savatenkov, V.M. (2015) Late Mesozoic–Cenozoic intraplate magmatism in Central Asia and its relation with mantle diapirism: Evidence from the South Khangai volcanic region, Mongolia. Journal of Asian Earth Sciences, 111, 604–623.

Zhang, Y.Y., Yuan, C., Sun, M., Chen, M., Hong, L.B., Li, J., Long, X.P., Li, P.F., and Lin, Z.F. (2019) Recycled oceanic crust in the form of pyroxenite contributing to the Cenozoic continental basalts in central Asia: New perspectives from olivine chemistry and whole-rock B–Mo isotopes. Contributions to Mineralogy and Petrology, 174, 1–22.

Zhao, D.P. (2004) Global tomographic images of mantle plumes and subducting slabs: insight into deep Earth dynamics. Physic of the Earth and Planetary Interiors, 146, 3–34.

Zhu, R.X., and Zheng, T.Y. (2009) Destruction geodynamics of the North China Craton and its Paleoproterozoic plate tectonics. Chinese Science Bulletin, 54, 3354–3366.

FIGURE CAPTIONS:

Figure 1. (a) Tectonic setting of the central Asia in the context of India–Eurasia collision (after Vassallo et al. 2007). Abbreviations: AT (Altyn Tagh); BR (Baikal Rift); DL (Mongolian Depression of Lakes); GA (Gobi Altai); HD (Hangai Dome); HR (Hövsgöl Rift); KS (Kunlun Shan); MA (Mongol Altai); QS (Qilian Shan); TS (Tian Shan). (b) Digital topography of central Asia (original data from Earth Remote Sensing Data Analysis Center, downloaded from https://earthexplorer.usgs.gov). The dark grey color shows the distribution of late Cenozoic volcanism in central Asia.

Figure 2. Geological map of the Hangai region showing the distribution and ages of Cenozoic basalts (after Ancuta et al. 2018). Cyan triangles indicate the localities where basaltic samples were studied here. VG stands for the Vodorazdel'nyi graben.

Figure 3. Optical images (crossed nicols), back-scattered electron images (with dotted electron probe microanalysis paths), and compositional traverses for representative olivine xenocrysts from samples 17MG58, 17MG65 and 17MG86 of the Cenozoic basalts in central Mongolia.

Figure 4. (a) Total alkali–silica (TAS) diagram (after Le Bas et al. 1986). BTA and TB represent basaltic trachyandesite and trachybasalt, respectively. (b) CaO versus MgO diagram. The darkgray area for peridotite partial melts and the green line separating pyroxenite from peridotite partial melts are from Herzberg and Asimow (2008). (c) FeO^T/MnO versus MgO diagram. The FeO/MnO range (grey field) for peridotite partial melts is from Herzberg (2011). (d) Primitive mantle-normalized trace element patterns for the Cenozoic basalts from central Mongolia. Normalizing values are from Sun and McDonough (1989). Previous data for the Jargalant, Tariat, Togo and Orkhon basalts are from Barry et al. (2003), Hunt et al. (2012) and Ancuta et al. (2018). Trace element compositions of peridotite xenoliths from the Tariat basalts are from Ionov et al. (1994).

Figure 5. (a) $^{143}Nd/^{144}Nd$ versus $^{87}Sr/^{86}Sr$ diagram. Previous data for the Orkhon, Tariat and Togo basalts are from Barry et al. (2003) and Hunt et al. (2012). The field for the Vitim mantle xenoliths is after Ionov et al. (1995), and the data for clinopyroxenes from the Hangai mantle xenoliths are from Stosch et al. (1986) and Ionov et al. (1994), and the data for the Hangai crustal xenoliths are from Barry et al.

(2003). (b) εHf versus εNd diagram. The evolution paths of GLOSS and oceanic crust are calculated following the approach of Chauvel et al. (2008), and the boundary of Nd–Hf isotopic compositions between the Indian and Pacific Ocean mantle domains is from Pearce et al. (1999).

Figure 6. Plots of Fo versus Ca (a–b), Mn (c–d) and Ni (e–f) in olivines of Cenozoic basalts in central Mongolia analyzed by EPMA. The calculated Ca, Mn and Ni compositions of olivines crystallized from peridotitic melts are from Herzberg (2011). The olivine data for N-MORB from Siqueiros are from Sobolev et al. (2007) and Putirka et al. (2011). Data of olivines in komatiites worldwide are from Sobolev et al. (2007), and data of olivines in EI Hierro basanites and La Palma picrobasalts are from Gurenko et al. (2009). The field for mantle olivines is based on data from Sobolev et al. (2009) and De Hoog et al. (2010).

Figure 7. Plots of Fo versus Li (a), P (b), V (c), Zn (d), Sc (e), Co (f), Cu (g) and Cr (h) in olivines of Cenozoic basalts in central Mongolia analyzed by LA-ICP-MS. Also shown are the corresponding compositions of mantle olivines (De Hoog et al. 2010).

Figure 8. Whole-rock Mg# versus Fo contents of olivine crystals in the Cenozoic basalts from central Mongolia. The Fe/Mg exchange partition coefficient between olivine and basaltic melt varies from 0.3 at 1 atm (Roeder and Emslie 1970) to 0.31–0.34 at 5–15 kbar (Ulmer 1989).

Figure 9. Relationships of Zn/Mn (a) and 10000*Zn/Fe (b) ratios with MgO contents for the Cenozoic basalts from central Mongolia. Peridotite ranges are from Le Roux et al. (2010). Previous data for the Jargalant, Tariat, Togo and Orkhon basalts are from Hunt et al. (2012) and Ancuta et al. (2018). Plots of (c) Mn versus Mn/Zn and (d) 100*Mn/Fe versus 10000*Zn/Fe for olivines in the studied Cenozoic basalts. The dashed line separating pyroxenite (Mn/Zn < 14) from peridotite (Mn/Zn > 14) sources in (c) is from Howarth and Harris (2017). The peridotite and pyroxenite ranges in (d) are from Sobolev et al. (2007) and Howarth and Harris (2017).

Figure 10. (a) Estimated mantle melting temperatures for the Cenozoic basalts in central Mongolia are plotted on the temperature axis. The lherzolite solidus is calculated by the parameterization of Katz et al. (2003), while the pyroxenite solidus is calculated using the model of Lambart et al. (2016) based on compositions of the silica-deficient pyroxenite M5-40. The geotherm for the Hangai (Tariat) region is after Ionov (2002), and the equilibrium P–T ranges for the Hangai peridotite xenoliths are from Harris et al. (2010). The spinel to garnet lherzolite transition and spinel to garnet pyroxenite transition are from O'Neill (1981) and Herzberg (1978), respectively. (b) Diagram of oxygen fugacity (△FMQ) versus Mn/Zn (olivine). Increasing oxygen fugacity with decreasing Mn/Zn may reflect the contribution of pyroxenite.

Figure 11. Schematic cartoon illustrating the formation process of Cenozoic basalts

This is the peer-reviewed, final accepted version for American Mineralogist, published by the Mineralogical Society of America.
The published version is subject to change. Cite as Authors (Year) Title. American Mineralogist, in press.
DOI: https://doi.org/10.2138/am-2020-7431. http://www.minsocam.org/

and the mechanism of Cenozoic regional uplift in the Hangai Mountains from central Mongolia. The primitive basaltic melts were formed in the upwelling asthenosphere by melting of secondary pyroxenite. When such melts ascended, they may assimilate the overlying mantle lithosphere, finally generating the studied basalts. On the other hand, melt–rock interaction in the mantle lithosphere could change the rheology and accelerate the erosion of mantle lithosphere. As a consequence, mass deficit in the lithosphere could have caused the Cenozoic isostatic uplift in the Hangai Mountains.


90°E
95°E
100°E
105°E
110°E
115°E
120°E
50°N
45°N
40°N
(b)
Vitim
Baikal Rift
Southwest Baikal
Mongol-Chinese Altai
Hangai Mountains
Ulaan Baatar
Dariganga
Fig.2
Gobi Altai
3000m
0m
0
200
400
600 km
(a)
Major fault
Thrust
Normal
Strike-slip
Fig.1b
RUSSIA
BR
HR
MONGOLIA
MA
DL
HD
GA
TS
QS
AT
KS
TIBET
CHINA
HIMALAYA
~4 cm/yr
INDIA
1000 km
N

Figure 1


E98°
E99°
E100°
E101°
E102°
E103°
E104°
N50°
N49°
N48°
N47°
N46°
24.5–26.1 Ma
11.3–12.3 Ma
Selenga River
5.7–5.9 Ma
Togo
Hanui
0.3 Ma
5.8 Ma
4.0–4.2 Ma
Orkhon
3.1–3.8 Ma
3.1 Ma
Tariat
Chulut River
Sumyn River
0.1–0.5 Ma
5.9 Ma
Hanui River
Orkhon River
10.5 Ma
15.7 Ma
13.7–14.0 Ma
13.4 Ma
Hangai
Mountains
Jargalant
Xoid Tamirin
7.5–9.7 Ma
6.0–12.8 Ma
7.4–9.2 Ma
VG
2.5–4.7 Ma
Nuruu
16.4–19.8 Ma
2.3–4.1 Ma
0.25 Ma
19.0–21.9 Ma
14.6–15.0 Ma
11.7–11.8 Ma
13.2–13.4 Ma
Sample location
0–5 Ma
5–10 Ma
10–15 Ma
15–20 Ma
20–25 Ma
25–30 Ma

Figure 2

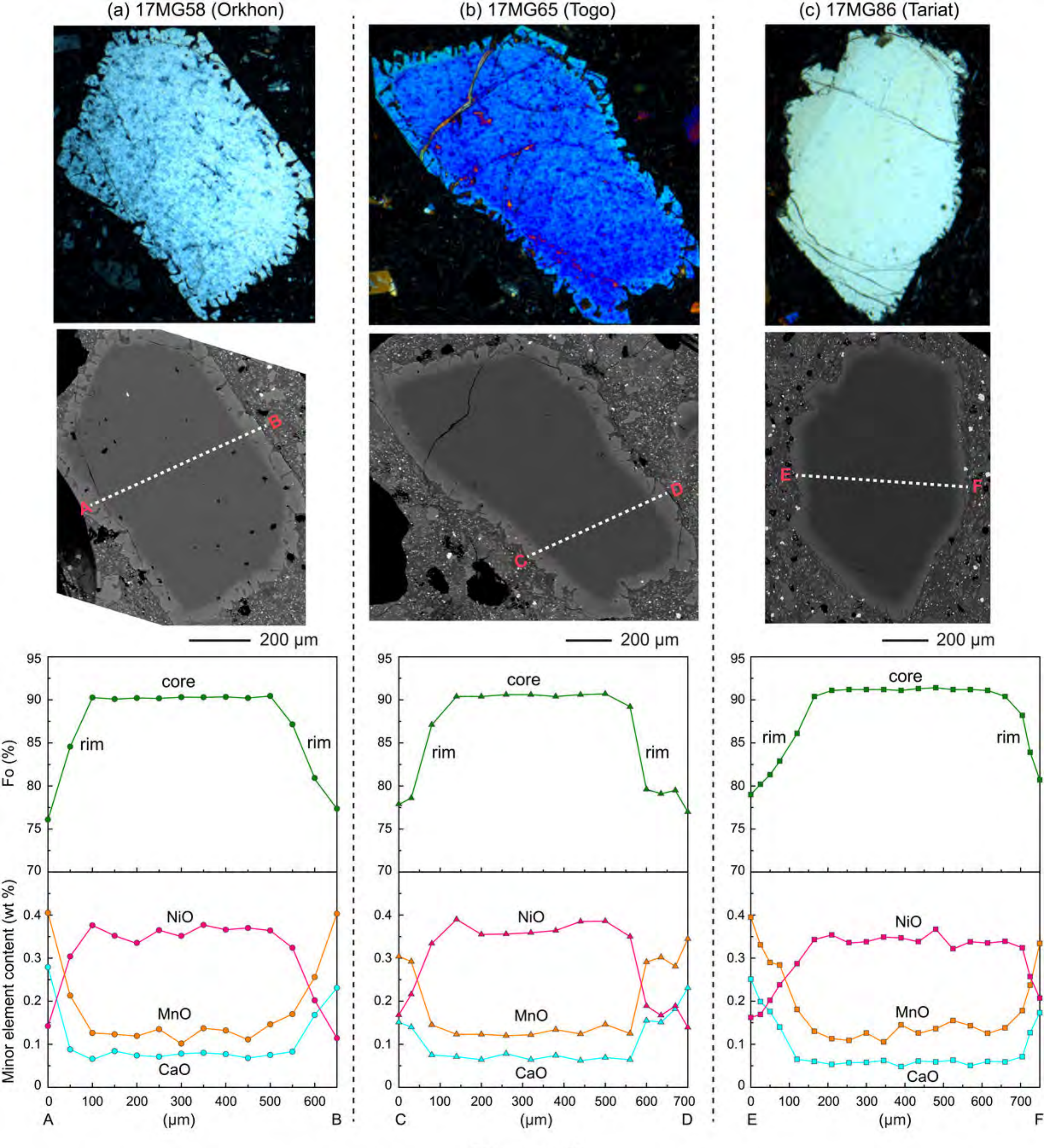

(a) 17MG58 (Orkhon)
(b) 17MG65 (Togo)
(c) 17MG86 (Tariat)
A
B
C
D
E
F
200 μm
core
rim
Fo (%)
NiO
MnO
CaO
Minor element content (wt %)
(μm)

Figure 3

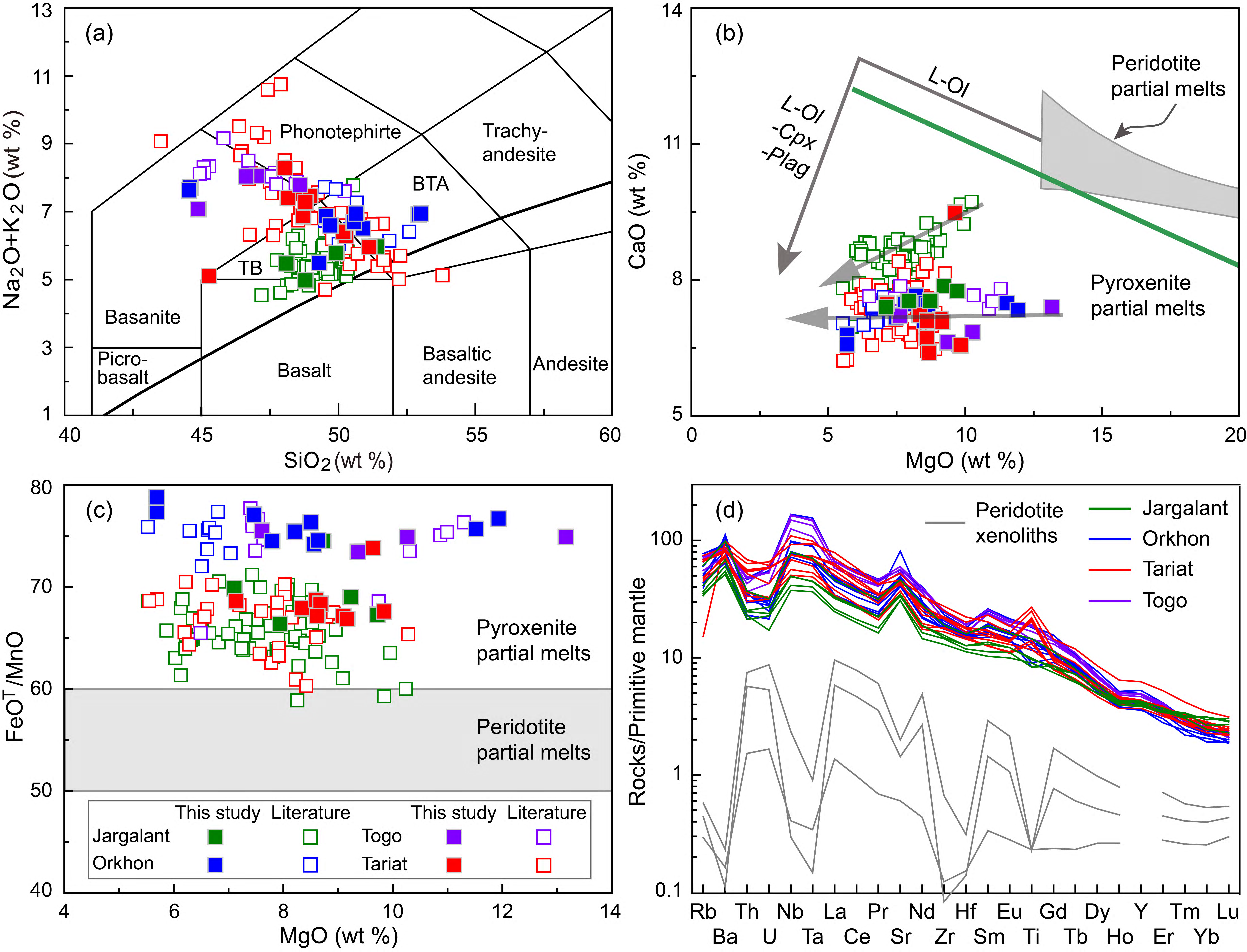
(a)
Phonotephirte
Trachy-
andesite
BTA
TB
Basanite
Picro-
basalt
Basalt
Basaltic
andesite
Andesite
Na_2O+K_2O (wt %)
SiO_2 (wt %)
(b)
L-Ol
L-Ol
-Cpx
-Plag
Peridotite
partial melts
Pyroxenite
partial melts
CaO (wt %)
MgO (wt %)
(c)
Pyroxenite
partial melts
Peridotite
partial melts
FeO^T/MnO
MgO (wt %)
This study
Literature
Jargalant
Orkhon
Togo
Tariat
(d)
Peridotite
xenoliths
Jargalant
Orkhon
Tariat
Togo
Rocks/Primitive mantle
Rb
Ba
Th
U
Nb
Ta
La
Ce
Pr
Sr
Nd
Zr
Hf
Sm
Eu
Ti
Gd
Tb
Dy
Ho
Y
Er
Tm
Yb
Lu

Figure 4

0.5135
0.5131
0.5127
0.5123
0.5119
^{143}Nd/^{144}Nd
0.702
0.704
0.706
0.708
0.710
^{87}Sr/ ^{86}Sr
Vitim mantle xenoliths
DMM
Cpx from 'dry' mantle peridotite (Hangai region)
Cpx from phlogopite mantle peridotite (Hangai region)
Hangai crustal xenoliths
EM-1
EM-2
(a)
This study
Literature
Jargalant
Orkhon
Togo
Tariat
20
10
0
-10
-20
-30
εHf
-25
-20
-15
-10
-5
0
5
10
εNd
GLOSS evolution through time (Ga)
Oceanic crust evolution through time (Ga)
Indian
Pacific
0.3
0.5
1.0
2.0
10
20
30
40
50
60
70
80
90
5
1
(b)

Figure 5

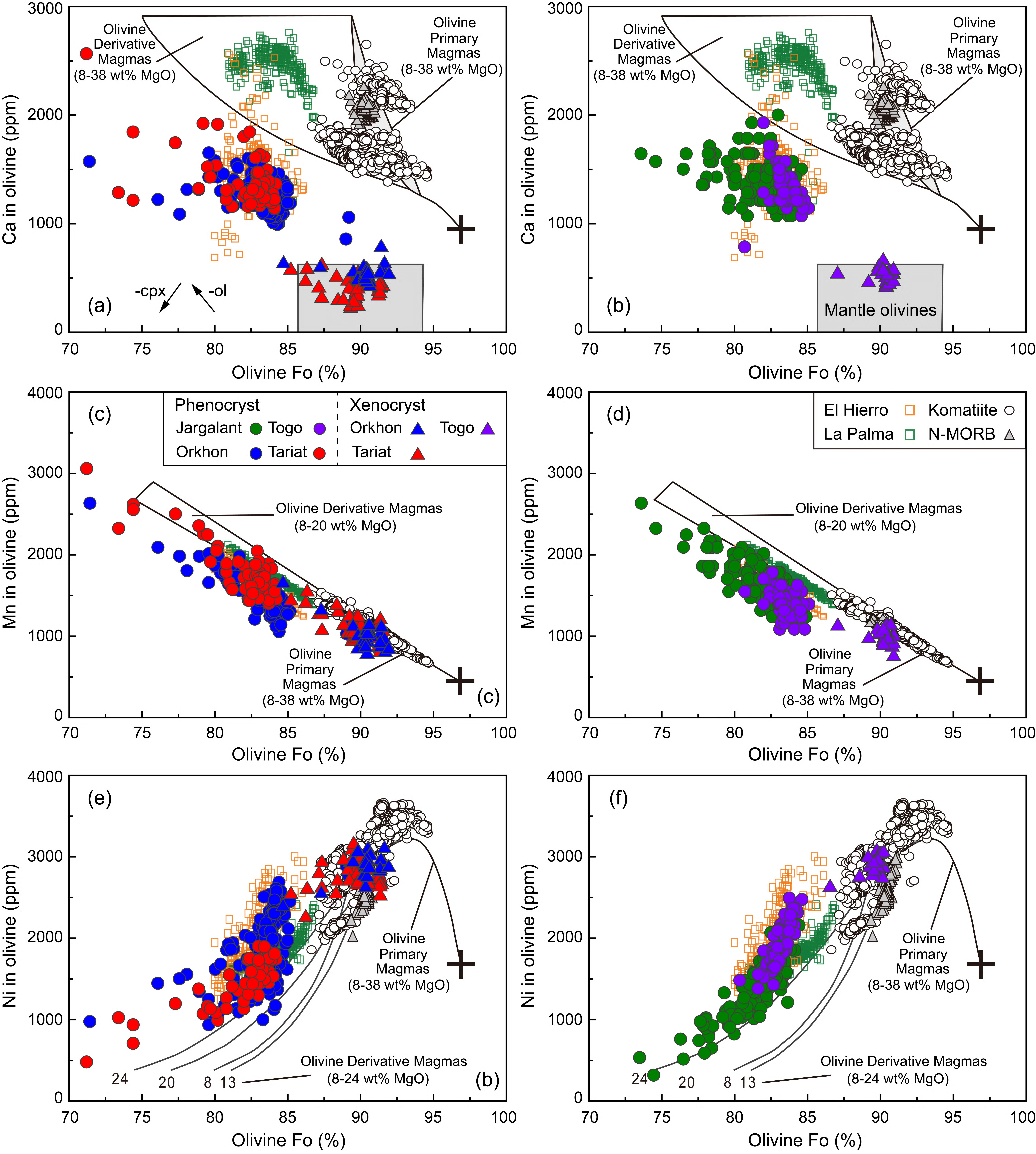

Olivine Derivative Magmas (8-38 wt% MgO)
Olivine Primary Magmas (8-38 wt% MgO)
Ca in olivine (ppm)
Olivine Fo (%)
-cpx
-ol
(a)
(b)
Mantle olivines
(c)
(d)
Phenocryst
Jargalant
Togo
Orkhon
Tariat
Xenocryst
Orkhon
Togo
Tariat
El Hierro
Komatiite
La Palma
N-MORB
Mn in olivine (ppm)
Olivine Derivative Magmas (8-20 wt% MgO)
(e)
(f)
Ni in olivine (ppm)
Olivine Derivative Magmas (8-24 wt% MgO)
24
20
8
13

Figure 6

Phenocryst
Jargalant
Togo
Orkhon
Tariat
Xenocryst
Orkhon
Togo
Tariat
Mantle olivines
(De Hoog et al., 2010)
Li in olivine (ppm)
Zn in olivine (ppm)
Co in olivine (ppm)
Sc in olivine (ppm)
Cr in olivine (ppm)
V in olivine (ppm)
Cu in olivine (ppm)
Ti in olivine (ppm)
P in olivine (ppm)
Olivine Fo (%)
(a)
(b)
(c)
(d)
(e)
(f)
(g)
(h)
(i)

Figure 7

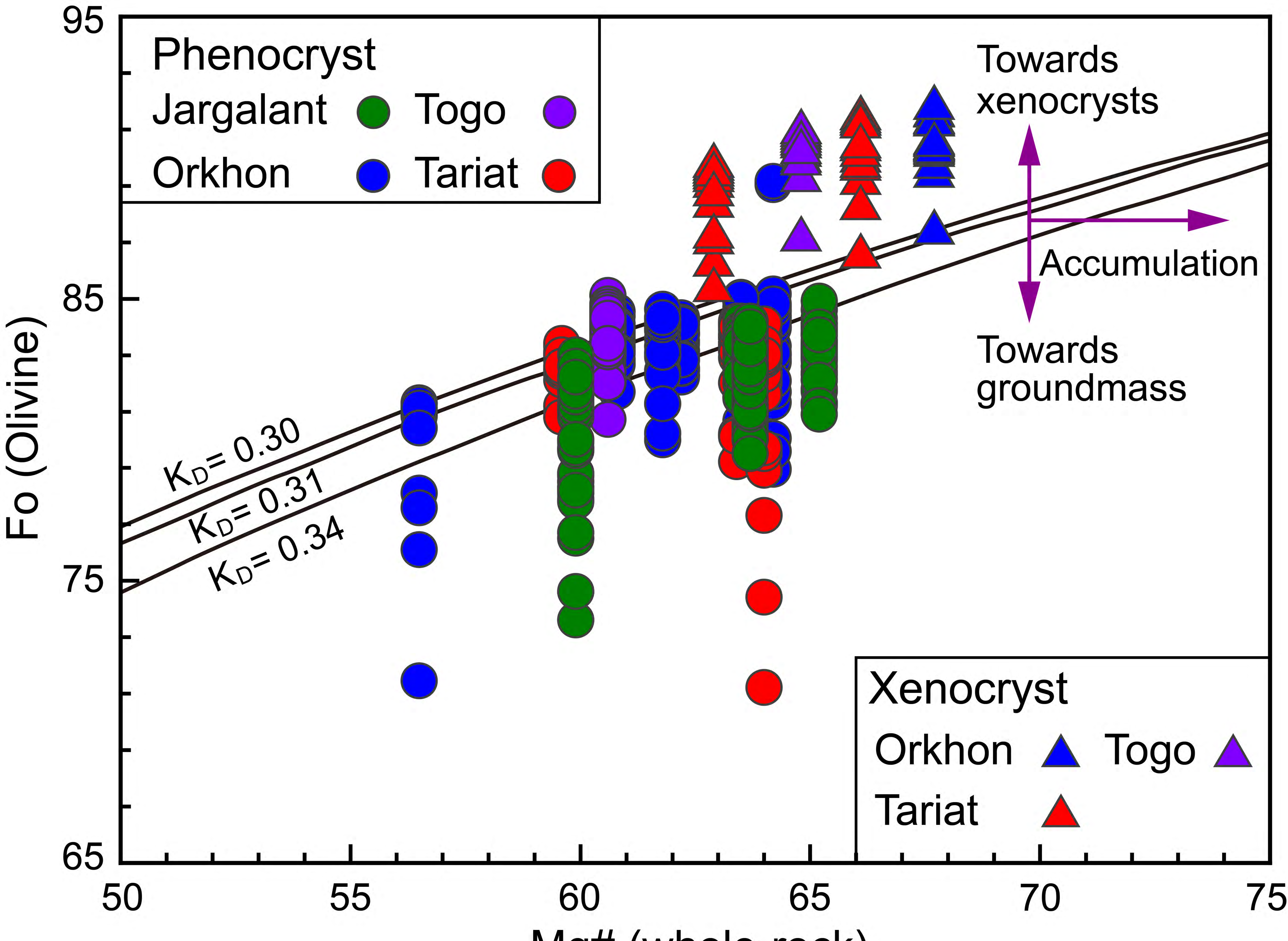
Phenocryst
Jargalant
Togo
Orkhon
Tariat
Towards xenocrysts
Accumulation
Towards groundmass
K_D= 0.30
K_D= 0.31
K_D= 0.34
Xenocryst
Orkhon
Togo
Tariat
Fo (Olivine)
Mg# (whole-rock)
95
85
75
65
50
55
60
65
70
75

Figure 8


(a)
WR Zn/Mn
WR MgO (wt %)
Peridotite range
This study
Literature
Jargalant
Orkhon
Togo
Tariat
(b)
WR Zn/Fe*10^4
WR MgO (wt %)
Peridotite range
(c)
Mn in olivine (ppm)
Mn/Zn in olivine
Peridotite source
Pyroxenite source
Jargalant
Orkhon
Togo
Tariat
(d)
100*Mn/Fe in olivine
10000*Zn/Fe in olivine
Peridotite
Pyroxenite

Figure 9

Temperature (°C)
900
1000
1100
1200
1300
1400
1500
1600
(a)
Sp→Gt pyroxenite
Sp→Gt lherzolite
Geotherm
TP = 1450°C
TP = 13000°C
Presure (GPa)
0
1
2
3
4
5
Lherzolite solidus
Pyroxenite solidus
Hangai peridotite xenoliths
Jargalant
Togo
Orkhon
Tariat
(b)
Jargalant
Togo
Orkhon
Tariat
Increasing pyroxenite?
Oxygen fugacity (ΔFMQ)
0.7
0.4
0.1
-0.2
-0.5
6
7
8
9
10
11
12
13
Mn/Zn in olivine

Figure 10


Hangai Mountains
Depth (km)
0
45
100
Crust
Lithospheric mantle
Asthenosphere
Basalt
Isostatic uplift
Olivine xenocryst
Melt-rock interaction
Melt
Mechanical and chemical erosion of mantle lithosphere
Upwelling asthenosphere

Figure 11